Title

Understanding the role of water-soluble guar gum binder in reducing capacity fading and voltage decay of Li-rich cathode for Li-ion batteries

Authors

Yin, Zu-Wei
Zhang, Tao
Zhang, Shao-Jian
et al.

Publication Date

2020-08-01

DOI

10.1016/j.electacta.2020.136401

Peer reviewed

Understanding the Role of Water-Soluble Guar Gum Binder in Reducing Capacity Fading and Voltage Decay of Li-rich Cathode for Li-Ion Batteries

Zu-Wei Yin[†,∥,#], Tao Zhang[†,#], Shao-Jian Zhang[†], Ya-Ping Deng[†], Xin-Xing Peng[‡,∥], Jian-Qiang Wang[§], Jun-Tao Li[†,*], Ling Huang[‡], Haimei Zheng [⊥], and Shi-Gang Sun[†,‡,*]

[†] College of Energy, Xiamen University, Xiamen 361005, China

[‡]State Key Lab of Physical Chemistry of Solid Surface, College of Chemistry and Chemical Engineering, Xiamen University, Xiamen 361005, China

[∥]Materials Sciences Division, Lawrence Berkeley National Laboratory, Berkeley, California 94720, United States

[⊥]Department of Materials Science and Engineering, University of California, Berkeley, California 94720, United States

[§]Shanghai Synchrotron Radiation Facility, Chinese Academy of Sciences, Shanghai 201204, China

* E-mail: jtli@xmu.edu.cn (J. T. Li), sgsun@xmu.edu.cn (S. G. Sun).

Abstract

The practical application of high-capacity Li-rich cathode materials is hindered by capacity fading and voltage decay. The capacity fading and voltage decay could be effectively overcome by using water-soluble guar gum (GG) binder instead of traditional polyvinylidene fluoride (PVDF). However, the specific role of the GG binder is not clear yet, though the GG binder can significantly improve the electrochemical performance of Li-rich cathode. To understand the effect of GG binder on the morphology, microstructure of electrode and electrode/electrolyte interfaces, *ex*-situ scanning electron microscope (SEM), transmission electron microscope (TEM), X-ray adsorption near edge spectroscopy (XANES), in-situ electrochemical impedance spectroscopy (EIS) were applied to comparatively study the charge-discharge processes of $Li_{1.2}Ni_{0.2}Mn_{0.6}O_2$ cathode when using GG and PVDF as binders. The results indicate that the GG binder can prevent electrode crack and active material loss, ascribing to the strong mechanical adhesion of GG binder with active material particles and current collector. It has found that the GG binder can also induce the formation of a uniform layer on $Li_{1.2}Ni_{0.2}Mn_{0.6}O_2$ particles' surface. As a consequence, both the electrolyte decomposition and the electrode corrosion were significantly inhibited. The strong chelation between Mn^{2+} and polar OH group restrain Mn ion dissolution, which contributes to surface structural transformation mitigation. The present study reveals the role of water-soluble GG binder in reducing capacity fading and voltage decay of Li-rich material and

is of great importance in design functional binders for high-performance Li-rich electrodes.

Key words: Lithium ion batteries, Li-rich material cathode, water-soluble binder, in-situ and ex-situ techniques, capacity fading, voltage decay

1. Introduction

Recently, the low available specific capacity of the traditional cathode materials such as $LiCoO_2$, $LiMn_2O_4$, and $LiFePO_4$ is becoming a bottleneck to the increase of the energy densities of the lithium-ion batteries (LIBs) for electric vehicles and electricity grid.[1-2] Layered Li-rich oxide cathode materials exhibit specific capacity of over 250 mAh g^{-1}, and thus they are potential candidates of next-generation LIBs cathode.[3] However, they suffer from severe capacity fading and voltage decay during cycling process, which induce energy density degradation and hinder their commercial application.[4-5]

For capacity fading, it can be solved by element doping, surface modification and structure regulation etc.[6-9] For example, doping with Al, Mg, Fe,[6] coating with TiO_2, ZrO_2, $AlPO_4$,[7] and regulation of particle size,[8] structure defects[9] are efficient to eliminate the capacity fading of Li-rich material. For voltage decay, it can be partially mitigated by doping or structure modulation.[10-11] Conventional coating with metal oxides has been proved having minimal effect on voltage decay.[8] The voltage decay mitigation by functional coating such as $LiFePO_4$[36] and Li-Mg-PO_4[37] was attributed to doping of core Li-rich materials caused by surface modification. But all these methods required complicated material preparation

processes.

Apart from the methods for material modifications, many functional water-soluble binders have been adopted to reduce capacity fading of both anode and cathode materials, which is much simpler than other methods such as element doping, surface modification and structure regulation etc.[12] For Li-rich materials, carboxymethyl cellulose (CMC),[13] sodium carboxymethyl cellulose (CMC-Na),[14] sodium alginate (SA),[15] and fluorine acrylic hybrid latex[38] have been successfully applied to alleviate its capacity fading and voltage decay. But the mechanism has not been studied,[38] or simply attributed to the resulted homogenous morphology,[13] binder induced Na^+ dopping,[14] and Mn ion dissolution inhibition.[15] The Mn ion dissolution inhibition was concluded from X-ray Photoelectron Spectroscopy (XPS),[15] which can only obtain the surface information of materials. Guar gum (GG), a natural nonionic polysaccharide extracted from the seeds Cyamopsis tetragonolobus, has strong mechanical property, good ion-conductivity and a large amounts of polar hydroxyl groups.[16] Our previous studies exhibit that such water-soluble GG could remit the capacity fade of Si anode and Li-S battery efficiently.[16-17] Guar gum was also applied in Li-rich oxide cathode material for the first time by our group. We found that GG can reduce the capacity fading and voltage decay of Li-rich material in the same time.[18] However, the mechanism of guar gum binder mitigating the capacity fading and voltage decay is not clarified clearly. The voltage decay of Li-rich materials is always attributed to layered-to-spinel phase transformation (surface and bulk).[19]

While the bulk phase transformation are possibly inhibited using doping or structure regulation methods,[10-11,14-15] surface phase transformation can be potentially mitigated using unique surface treatment methods.[19-20, 36-37] The extraordinary voltage decay mitigation by GG binder makes it attractive to reveal the specific role of water-soluble GG binder.

Here, we compared the electrochemical performance, morphology, microstructure, valence state and local structure of Mn element, and electrode/electrolyte interfacial properties of $Li_{1.2}Ni_{0.2}Mn_{0.6}O_2$ cathode materials during cycling using polyvinylidene fluoride (PVDF) or guar gum (GG) as binder. The results demonstrate that GG binder can reduce the capacity fading and voltage decay of Li-rich material obviously, which is caused by preventing the crack of electrode, reducing active material loss and side reactions at electrode/ electrolyte interfaces, limiting surface structural transformation of Li-rich material. The mechanism of GG binder alleviating voltage and capacity fading could be ascribed to its participating to form more stable cathode electrolyte interphase (CEI) on surface of $Li_{1.2}Ni_{0.2}Mn_{0.6}O_2$ particles and strong chelation with Mn ions.

2. Experimental

2.1. Synthesis

A molten salt method was used to synthesize the $Li_{1.2}Ni_{0.2}Mn_{0.6}O_2$ cathode

materials. A large excess of KCl salt and a stoichiometric amount of Li_2CO_3, $Ni(CH_3COO_2)\bullet 4H_2O$, $Mn(CH_3COO_2)\bullet 4H_2O$ were mixed by ball milling. The prepared mixture by milling was then put in tube furnace to calcine in air (450℃ for 6 h and then 800 ℃ for 12 h). The obtained product was washed using deionized water for several times to remove the residual KCl salt. Subsequent filtration was conducted, and it was then dried at 100 ℃for 10 h. The specific preparation process of samples can be seen in our previous studies.[21]

2.2. Characterization

SEM (Hitachi S-4800) and TEM (JEOL JEM-2100F) were applied to examine the morphology and microstructure. X-ray diffraction (XRD, Philips X'Pert Pro) was used to characterize the crystal structure in the 2θ range of 15-75º with a scan rate of $1º\cdot min^{-1}$. Ex-situ XANES was conducted at the BL14W1 beamline on Shanghai Synchrotron Radiation Facility (SSRF). All the thin-film $Li_{1.2}Ni_{0.2}Mn_{0.6}O_2$ electrodes for XANES measurements were assembled in an Ar filled glovebox using CR2025-type coin cells, on which surface a hole of 3 mm in diameter was drilled and sealed with Kapton membrane. The prepared thin-film $Li_{1.2}Ni_{0.2}Mn_{0.6}O_2$ electrodes were obtained by disassembling the cells at different cut-off voltages or after different cycles. Dimethyl carbonate (DMC) was used to wash the electrodes.

2.3. Electrochemical tests

CR2025-type coin cells were applied to do electrochemical tests. Slurries of synthesized material, acetylene black and binder (polyvinylidenediuoride (PVDF) or guar gum (GG)) at a weight ratio of 80: 10: 10 were prepared. N-methyl-2-pyrrolidone (NMP) and deionized water was used as solvent when PVDF and GG was used as binder, respectively. The obtained slurries were coated on Al foil current collector with the diameter of 16 mm and then dried at 100 °C for 12 h in vacuum. The active material mass loading was kept at 1.2±0.1 mg cm^{-2}. The CR2025-type coin cells were assembled in an Argon-filled glove box. A lithium foil was used as both counter and reference electrode. A Celgard2400 film was used as separator and 1 M $LiPF_6$ dissolved in ethylene carbonate (EC)/dimethyl carbonate (DMC) (1:1 v/v) as electrolyte. The cells were charged-discharged galvanostatically on a Land-V34 battery tester (Wuhan, China) at 30 ^{o}C. The current density of 1 C equals to 200 mA g^{-1}. The test voltage region of all the cells is 2.0-4.8 V (*vs*. Li/Li^{+}). The capacities were calculated based on the weight of active material.

Cyclic voltammetry (CV) curves were conducted using two kinds of electrodes. One is the same as the coin cells for charge-discharge tests. The other one is only PVDF or GG binder and carbon black on Al foil current collector. The binder mass loading was kept at 0.15±0.02 mg cm^{-2}, which is 10% of the whole loading mass of the cells for charge-discharge tests. The mass ratio of PVDF/GG binder to carbon black is 1:1. The applied range was 2.0-4.8 V and scanning rate was 0.2 mV s^{-1}. The current density was calculated based on loading mass of

binders.

Electrochemical impedance spectroscopy (EIS) measurements were performed using a VSP multichannel potentiostatic-galvanostatic system (VERSASTATV3, USA). An AC voltage of 5 mV and a frequency range of 1 MHz-5 mHz were applied. For in-situ EIS, the electrode potential was increased stepwise from open circuit voltage (OCP) to 4.8 V with 0.1-0.2 V potentiostatic steps. Before EIS tests at each potential, this voltage was kept constant for 20 min. The EIS results were fitted using Zview software.

3. Results and Discussion

The XRD pattern of $Li_{1.2}Ni_{0.2}Mn_{0.6}O_2$ material was displayed in Fig. S1, which has the evident feature of layered structure. The major peaks (such as 18.7° and 44.6°) are indexed to α-$NaFeO_2$ parent hexagonal phase ($R\acute{3}m$ space group). A broad super-lattice peak at 20-25° indicates the monoclinic structure of Li_2MnO_3 component (C2/m).[22] Fig. 1a demonstrates the initial charge/discharge profiles of $Li_{1.2}Ni_{0.2}Mn_{0.6}O_2$ at 0.2 C using PVDF or GG as binder. For first charge, the electrodes using PVDF and GG binder show similar curve at the voltage region of ¿4.65 V. It includes a typical sloping curve at the voltage region of ¿4.5 V and a steady plateau at ~4.5 V, which is caused by Ni^{2+}/Ni^{4+} redox and activation of Li_2MnO_3 component respectively.[1-2] In the region ¿4.65 V, the electrode using PVDF binder shows a higher capacity of 72 mAh g^{-1} than that of

42 mAh g^{-1} using GG binder. The capacity at high voltage is always attributed to side reactions originated from electrolyte decomposition.[23] The lower charge capacity in the region of ¿4.65 V using GG binder indicates that GG can inhibit the side reactions at high voltage. For first discharge, the electrodes using PVDF and GG binder show the almost same curve shape and similar capacity of 238 mAh g^{-1} and 240 mAh g^{-1}. The CV curves of $Li_{1.2}Ni_{0.2}Mn_{0.6}O_2$ material using PVDF or GG binder are shown in Fig. S2. It can be observed that the electrode using GG binder exhibits a slightly lower current density than that using PVDF binder at high charge voltage, but almost no difference during discharge. The results of CV are consistent with that of the initial charge/discharge curves.

To further explore the role of GG binder in inhibiting electrolyte side reactions, the CV curves of electrodes only consisting of PVDF or GG binder on Al current collector were depicted in Fig. 1b. It is obvious that electrode with GG binder shows a much lower electrolyte oxidation current. For discharge, both electrodes with PVDF and GG binder display negligible reduction current. The electrolyte oxidation is affected by the surface properties of electrode, which was reported in both experimental and theoretical studies.[24-25] Our results indicate that GG binder is more inactive than PVDF and Li-rich material for electrolyte oxidation. Using GG binder can inhibit the side electrolyte decomposition reactions at high voltage.

Fig. 1c exhibits the cyclability of $Li_{1.2}Ni_{0.2}Mn_{0.6}O_2$ at 0.5 C using PVDF or GG as

binder, and the corresponding average discharge voltages were demonstrated in Fig. 1d. The initial capacity of PVDF and GG using as binder is similar 187 mAh g^{-1} and 186 mAh g^{-1}, respectively. But when using GG as binder, the capacity can possess retention of 95.3% after 200 cycles, which is distinctly higher than that of 73.1% using PVDF as binder. The initial average discharge voltage is similar 3.43 and 3.48 V for electrodes with PVDF and GG binder, respectively. But after 200 cycles at 0.5 C, the retention of average discharge voltage is 90.2% for electrode using GG as binder, while that for electrode using PVDF binder is only 80.8%. More detailed discharge curves at 0.5 C for different cycles were exhibited in Fig. S3a and b. It is distinct that electrode using PVDF binder has a more severe capacity fading and voltage decay than that using GG binder. Figure S4 displays the dQ/dV curves of $Li_{1.2}Ni_{0.2}Mn_{0.6}O_2$ electrodes using PVDF and GG binder. Liu's work displays similar dQ/dV curves of $Li_{1.2}Ni_{0.2}Mn_{0.6}O_2$ with and without NH_4F-Al_2O_3 surface co-modification.[41] $Li_{1.2}Ni_{0.13}Co_{0.13}Mn_{0.54}O_2$ with different binders also exhibits similar dQ/dV curves.[14] We observe in Figure S4 that, for first cycle, the peaks at 4.2 and 3.7 V correspond to Ni^{4+}/Ni^{2+} redox, and the peak at 3.25 V associates with Mn^{4+}/Mn^{3+} reduction.[41] During cycling, the Ni^{4+}/Ni^{2+} peaks of electrode using GG binder are more stable than that using PVDF binder. Both Mn^{4+}/Mn^{3+} peaks of electrodes using PVDF and GG binders demonstrate negative shift. Such a negative shift corresponds to layered-to-spinel phase transformation.[42] Spinel (i.e.$Li_xMn_2O_4$) has a distinct Mn^{4+}/Mn^{3+} reduction peak at 2.7 V,[43] which is much lower than the Mn^{4+}/Mn^{3+} peak of

layered Li-rich materials. It's reasonable that layered-to-spinel structural transformation leads to negative shift of Mn^{4+}/Mn^{3+} reduction peak. But the negative shift of electrode using PVDF (0.62 V) is much bigger than that using GG binder (0.37 V), providing a direct evidence that the GG binder can inhibit the layered-to-spinel phase transformation in comparison with PVDF binder.

To further explore the capacity and voltage stability of Li-rich cathode at different charge-discharge conditions, Fig. S3c shows the cyclability of $Li_{1.2}Ni_{0.2}Mn_{0.6}O_2$ at 1 C using PVDF or GG as binder, in which the first cycle was activated at 0.2 C. And the corresponding average discharge voltage was illustrated in Fig. S3d. When the charge-discharge rate increases from 0.2 C to 1 C at the second cycle, an obvious Ohmic polarization can be observed, which is caused by the increase of operation current.[44-45] Due to the higher internal resistance of electrode using PVDF (Figure 2) than that using GG binder, a 0.272 V higher IR drop of electrode using PVDF binder was exhibited (Fig. S3d). Excluding the first activation cycle at 0.2 C, the electrode using PVDF binder shows 59.1% capacity retention and 83.45% voltage retention after 200 cycles, while electrode using GG binder has a much higher 94.4% capacity retention and 95.2% voltage retention.

To further confirm the role of GG binder in mitigating interfacial reaction shown in Fig. 1a and b, we made a comparison of electrode/electrolyte interfacial properties between electrode with PVDF and GG binder (Fig. 2). Fig.

2a displays the Nyquist plots of $Li_{1.2}Ni_{0.2}Mn_{0.6}O_2$ before cycling using PVDF or GG as binder. The corresponding equivalent electric circuit at open circuit potential (OCP) is shown as insert. R_S and R_{CEI} represents the internal resistance and resistance of cathode electrolyte interface (CEI) film respectively. C_{CEI} represents the capacitance of the CEI film. W is the Warburg impedance related to Li^+ diffusion.[26] The R_{CEI} of electrode using PVDF binder (243.3 ohm) is much higher than that using GG binder (88.6 ohm) and the fitted data were listed in Table 1. There is always native Li_2CO_3 film on lithium transition metal oxides.[27] And the Li-rich materials can have chemical reactions with electrolyte even without charge-discharge,[27] which will increase the resistance of CEI film at the open circuit potential (OCP) state. The much smaller R_{CEI} at OCP state indicates that GG binder can protect the $Li_{1.2}Ni_{0.2}Mn_{0.6}O_2$ material from electrolyte. The reaction between $Li_{1.2}Ni_{0.2}Mn_{0.6}O_2$ material and electrolyte during storage is remitted by using GG binder. Similar phenomena were also observed for polar CN group based water-soluble binder.[28]

The evolution of R_{CEI} of $Li_{1.2}Ni_{0.2}Mn_{0.6}O_2$ at different first-charge potentials was shown in Fig. 2b, in which PVDF or GG binder was applied. Both R_{CEI} of electrodes using PVDF and GG binder display an initial decrease and subsequent increase trend, which indicates a native CEI film dissolution and subsequent electrolyte decomposition induced CEI film formation process.[27,29] However, the varied range of R_{CEI} for electrode using PVDF (211.8→116.1→223.2) is much bigger than that for electrode using GG binder (82.6→73.1→84.2), manifesting

the instability of electrode/electrolyte interface when using PVDF binder. The detailed EIS spectra during first charge were depicted in Fig. S5, including the enlarged R_{CEI} parts and whole frequency spectra. The specific fitted EIS results were listed in Table 1. To clarify the effect of GG binder on electrode/electrolyte interfaces of $Li_{1.2}Ni_{0.2}Mn_{0.6}O_2$ material during cycling, Nyquist plots of $Li_{1.2}Ni_{0.2}Mn_{0.6}O_2$ after different cycles at 0.5 C using PVDF or GG as binders are demonstrated in Fig. 2c and d. R_{CEI} of electrode using PVDF binder is evidently increased with cycle number (211.8→831.1). However, the R_{CEI} of electrode using GG binder almost keeps constant (82.6→86.4). The fitted impedance parameters were listed in Table 2. The similar phenomena were reported for protective layer induced by cathode additive, which can restrain the electrolyte decomposition and make interface resistance relatively stable.[30-31] From above, we observed that using GG binder can remit the electrolyte decomposition and stabilize the electrode/electrolyte interfaces.

Fig. 3 compares the morphology of $Li_{1.2}Ni_{0.2}Mn_{0.6}O_2$ electrodes with PVDF binder and GG binder. Fig. 3a and b show the SEM images of the $Li_{1.2}Ni_{0.2}Mn_{0.6}O_2$ cathodes before cycling. The differences between electrodes using PVDF binder and GG binder are insignificant and both of them show flat morphology. The SEM images of $Li_{1.2}Ni_{0.2}Mn_{0.6}O_2$ cathodes after 50 cycles at 0.5 C are exhibited in Fig. 2c and d. Cracks are observed on surface of electrode using PVDF binder, while the surface of electrode using GG binder keeps uniform. The cracks can lead to active material loss and worsen the electrochemical performance.[16]

PVDF could lose its adhesion with electrode particles gradually through absorbing electrolyte,[32] and the dehydrofluorination reaction of PVDF itself also induce degradation,[27] which is responsible for the peeling of active material. For GG binder, its strong adhesion, hydrogen bond with $Li_{1.2}Ni_{0.2}Mn_{0.6}O_2$ material and excellent mechanical properties make the electrode particles keep stable on current collector. The similar interaction between GG binder and Si anode, S cathode have been reported in our previous studies.[16-17]

Fig. 4 makes a microstructure comparison of $Li_{1.2}Ni_{0.2}Mn_{0.6}O_2$ particles after 50 cycles at 0.5 C with PVDF and GG binders. Before cycling, the pristine $Li_{1.2}Ni_{0.2}Mn_{0.6}O_2$ particles exhibit a smooth polyhedron shape with size of 150-200 nm (Fig. S6a), and a clean surface is observed (Fig. S6b). But after 50 cycles at 0.5 C, the structure of particle has obvious difference when different binders were applied. Many small isolated islands in the particle (Fig. 4a) and non-uniform species on the rough surface (Fig. 4b) can be seen when using PVDF as binder, which is attributed to the etching of acidic species from the electrolyte[33] and electrolyte decomposition[30-31]. Nevertheless, a smooth particle surface (Fig. 4c) and uniform coating layer (Fig. 4d) after cycling can be obtained when using GG as binder. The transparent feature (Fig. 4c and d) of such a uniform coating layer indicates that organic species is mainly composed, including GG binder and electrolyte decomposition product[18]. The uniform coating layer on Li-rich particles surface can prevent the further electrolyte decomposition and particles etching of electrolyte, which can contribute to the capacity retention, similar to

surface coating such as TiO_2, ZrO_2, $AlPO_4$.[7] However, these coatings produced little-to-no effect on voltage fading.[8] Some functional coatings such as $LiFePO_4$, Li-Mg-PO_4, CMC-Na binder were reported that can remit voltage decay, due to surface modification induced metal ion doping of core Li-rich materials.[14,37-38] For organic GG binder, C, H and O are the whole elements composed.[16-18] It is infeasible to induce doping by GG binder. And to the best of our knowledge, there is no reports that electrolyte decomposition produced CEI can induce bulk doping of particles.[30-31] A different mechanism for voltage decay mitigation by GG binder exists and needs further study.

To further investigate the effect of GG binder on structure evolution of Li-rich material, XANES was used to characterize the $Li_{1.2}Ni_{0.2}Mn_{0.6}O_2$ electrodes using PVDF or GG binder. XANES spectra is sensitive to the valence state and local environment of metal ions since a higher valence induced shorter bond length in the compound increases the absorption edge energy.[22] The valence state can be determined using the half-height and top-peak energies comparing with baseline sample.[22] Fig. S7 demonstrates the *ex*-situ Mn K-edge XANES spectra of $Li_{1.2}Ni_{0.2}Mn_{0.6}O_2$ before cycling, along with Mn_2O_3 (Mn^{3+}) and MnO_2 (Mn^{4+}) for a baseline study. It can be seen that the valence state of Mn in $Li_{1.2}Ni_{0.2}Mn_{0.6}O_2$ material is not ideal +4, but between +3 and +4, due to the materials loss during preparation process.[22]

The *ex*-situ Mn K-edge XANES spectra of $Li_{1.2}Ni_{0.2}Mn_{0.6}O_2$ during first cycle at

0.2 C using PVDF or GG as binder were depicted in Fig. 5. Fig. 5a and d demonstrate the whole spectra of $Li_{1.2}Ni_{0.2}Mn_{0.6}O_2$ using PVDF and GG binder respectively. Fig. 5b and c are local enlarged images of zone A and B in Fig. 5a, and Fig. 5e and f are local enlarged images of zone A and B in Fig. 5d. Positive shift of zone A during first charge indicates the activation of Li_2MnO_3 component.[22,34] And negative shift of zone A during first discharge manifests the phase transformation from layered structure to $Li_xMn_2O_4$-like spinel.[22,34] As exhibited in Fig. 5b and e, in the same scale, it is distinct that phase transformation in electrode using GG binder is milder than that using PVDF binder. Many studies suggested that the phase transformation from layered to spinel structure is responsible to voltage decay of Li-rich oxides.[19-20] The results are coincided with the electrochemical performance shown in Fig 1. Positive/negative shift of zone B indicates the oxidation/reduction of Mn element in $Li_{1.2}Ni_{0.2}Mn_{0.6}O_2$ material.[22,34] As depicted in Fig. 5c and f, all the spectra show an almost same half-height energy of 6556 eV. But in the scale, the Mn K-edge peak of electrode using PVDF binder has a 0.6 eV positive shift during first charge and 1 eV negative shift during first discharge, while that using GG binder shows almost invisible changes and only a total 0.1 eV positive shift after first cycle (Fig. 5f insert). It means the Mn valence state in $Li_{1.2}Ni_{0.2}Mn_{0.6}O_2$ using PVDF binder experienced a slight oxidation/reduction reaction during first cycle, while that using GG binder is stable.

To further verify the effect of GG binder on structural transformation of

$Li_2Ni_{0.2}Mn_{0.6}O_2$ material during cycling, *ex*-situ Mn K-edge XANES spectra of $Li_{1.2}Ni_{0.2}Mn_{0.6}O_2$ after different cycles at 0.5 C using PVDF or GG binders are exhibited in Fig. 6. Fig. 6a and d demonstrate the whole spectra of $Li_{1.2}Ni_{0.2}Mn_{0.6}O_2$ using PVDF and GG binder respectively. Fig. 6b and c are local enlarged images of zone A and B in Fig. 6a, and Fig. 6e and f are local enlarged images of zone A and B in Fig. 6d. There is an obvious phase transformation to form $Li_xMn_2O_4$-like spinel during cycling when used PVDF as binder (Fig. 6b). In the same scale, Fig. 6e indicates that the phase transformation is much slighter using GG binder, which is consistent with the results displayed in Fig. 5. Fig. 6c and f shows the Mn valence state change during cycling using PVDF and GG binder respectively. It can be observed that Mn valence state of electrode using PVDF binder keeps almost stable during cycling, while that using GG binder has a slight positive shift. For electrode using GG binder, it could be understood that the very slight Mn ion oxidation per cycle accumulated during cycling, then leads to visible positive shift of Mn K-edge. But for electrode using PVDF binder, Mn K-edge demonstrates a negative shift during first cycle (Fig. 5c). A negative shift of Mn K-edge is expected due to cycling accumulation. The abnormal stable Mn K-edge indicates that other Mn ion reactions take place during cycling. It is reported that disproportionation reaction ($2Mn^{3+} \rightarrow Mn^{2+} + Mn^{4+}$) can easily take place for spinel $LiMn_2O_4$ and the produced Mn^{2+} ions subsequently dissolve in the electrolyte.[35] The left Mn^{4+} will make the Mn valence state of $LiMn_2O_4$ slightly increase. So, the combination of Mn ion reduction and Mn ion dissolution can

potentially make the Mn valence state stable. The Mn^{3+} disproportionation reaction consumes the $Li_xMn_2O_4$-like spinel phase and can further promote the layered-to-spinel phase transformation. For water-soluble GG binder, our previous study proves that it can remit the Mn ion dissolution of cathode material for Na-ion batteries.[39] Previous study indicates that the strong chelation of Mn^{2+} by polar OH group in water-soluble alginate binder is responsible for the Mn^{2+} dissolution mitigation of $LiMn_2O_4$ cathode.[40] The Mn^{2+} dissolution restriction by GG binder facilitates to remit layered-to-spinel phase transformation, which further leading to voltage decay mitigation.

It should be mentioned that in our experiment adopting transmission mode, the XANES reflects the overall information of electrodes, including surface and bulk region. The obtained spectroscopic information of Mn element is an average value of whole electrode.[46] According to Gu's work,[19] there are two routes of layered-to-spinel transformation. The two different structures ($R\acute{3}m$ for $LiMO_2$ (M=Ni, Co, Mn), C2/m for Li_2MnO_3) follow different structural transformation routes during cycling. For the $R\acute{3}m$ structure, nucleation of spinel is from surface to bulk, which can be relieved by surface modifications (i.e. AlF_3 coating). While for the C2/m, the spinel grains dispersed in the whole particles, and the structural transformation of C2/m cannot be stopped by surface modifications. For the GG binder, similar to the reported surface modification methods,[19] it is reasonable that it can only inhibit the surface structural transformation. The structural transformation in the bulk make voltage decay

can be still observed during the cycling (Fig. 1d).

Based on the above results, Scheme 1 illustrates the different role of PVDF and GG binder in charge-discharge process of $Li_{1.2}Ni_{0.2}Mn_{0.6}O_2$ material. As depicted in Scheme 1, both PVDF and GG binder can bond with Li-rich particles and carbon black in the initial state and make them adhere with current collector. The Li-rich particles are exposed to electrolyte, including HF specie. But distinct difference can be observed during cycling when PVDF and GG was used as binder respectively. For PVDF binder, as illustrated in Scheme 1a, electrolyte decomposition takes place on particles surface, and HF etching with particles leads to a rough surface. In addition, severe voltage decay is caused by layered-to-spinel phase transformation (surface and bulk). The spinel suffers a disproportion reaction ($2Mn^{3+} \rightarrow Mn^{2+} + Mn^{4+}$) and subsequent Mn^{2+} dissolution, which further facilitate the phase transformation. For GG binder, a uniform layer on Li-rich particles surface was gradually produced (Scheme 1b). The further HF etching and electrolyte decomposition is prevented, which leads to a smooth and clean surface of Li-rich particles, resulting in good capacity retention. As a result of chelation between OH groups in GG binder and Mn^{2+}, the Mn^{2+} dissolution from produced spinel in surface region is also distinctly restrained by GG binder, which makes Mn ion accumulated in the particle/GG binder interface and inhibits the surface layered-to-spinel phase transformation, resulting in voltage decay mitigation.

4. Conclusions

In summary, the electrochemical performance, electrode/electrolyte interfaces, morphology, microstructure, valence state and local structure of Mn element of $Li_{1.2}Ni_{0.2}Mn_{0.6}O_2$ material was comparatively studied by applying PVDF or GG binder. The results have revealed the role of GG binder in reducing capacity fading and voltage decay of the Li-rich cathode. In comparison with PVDF binder, the GG binder has a strong adhesion effect with Li-rich material, preventing effectively the electrode crack and active material loss. More importantly, the GG binder facilitates the formation of a uniform protective layer on Li-rich particles surface, which provides a stable cathode electrolyte interphase (CEI) and alleviate the electrolyte decomposition and particles etching from electrolyte. The GG binder can also capture Mn^{2+} from Li-rich cathode, inhibiting Mn ion dissolution and surface layered-to-spinel phase transformation. Our study has advanced the understanding the charge-discharge mechanism of Li-rich materials and the interaction function of water-soluble binders with electrode. It promotes practical applications of Li-rich materials and the widespread use of water-soluble binders.

Author Information

Corresponding Author:

* E-mail: jtli@xmu.edu.cn (J. T. Li), sgsun@xmu.edu.cn (S. G. Sun).

Author contributions

[#] Z. W. Yin and T. Zhang contributed equally to this work.

Notes:

The authors declare no competing financial interest.

Acknowledgements

This work is supported by NSFC (21621091). Z. W. Yin acknowledges funding support from the China Scholarship Council (201606310151). H. Zheng thanks the support of U.S. Department of Energy (DOE), Office of Science, Office of Basic Energy Sciences (BES), Materials Science and Engineering Division under Contract No. DE-AC02-05-CH11231 within the KC22ZH program.

References

[1] Y. P. Deng, Z. G. Wu, R. Liang, Y. Jiang, D. Luo, A. Yu, Z. Chen, Layer-based heterostructured cathodes for lithium-ion and sodium-ion batteries, Adv. Funct. Mater. 29 (2019) 1808522.

[2] S. Hy, H. Liu, M. Zhang, D. Qian, B. J. Hwang, Y. S. Meng, Performance and design considerations for lithium excess layered oxide positive electrode materials for lithium ion batteries, Energy & Environ. Sci. 9 (2016) 1931-1954.

[3] E. McCalla, A. M. Abakumov, M. Saubanère, D. Foix, E. J. Berg, G. Rousse, M-L. Doublet, D. Gonbeau, P. Novák, G. Tendeloo, R. Dominko, J-M. Tarascon,

Visualization of OO peroxo-like dimers in high-capacity layered oxides for Li-ion batteries, Science 350 (2015) 1516-1521.
[4] M. Sathiya, A. M. Abakumov, D. Foix, G. Rousse, K. Ramesha, M. Saubanère, M. L. Doublet, H. Vezin, C. P. Laisa, A. S. Prakash, D. Gonbeau, G. VanTendeloo, J-M. Tarascon, Origin of voltage decay in high-capacity layered oxide electrodes, Nat. Mater. 14 (2015) 230.
[5] C. J. Chen, W. K. Pang, T. Mori, V. K. Peterson, N. Sharma, P. H. Lee, S. H. Wu, C-C. Wang, Y-F. Song, R. S. Liu, The Origin of capacity fade in the Li_2MnO_3· $LiMO_2$ (M= Li, Ni, Co, Mn) microsphere positive electrode: an operando neutron diffraction and transmission x-ray microscopy sudy, J. Am. Chem. Soc. 138 (2016) 8824-8833.
[6] P. K. Nayak, E. M. Erickson, F. Schipper, T. R. Penki, N. Munichandraiah, P. Adelhelm, H. Sclar, F. Amalraj, B. Markovsky, D. Aurbach, Review on challenges and recent advances in the electrochemical performance of high capacity Li- and Mn- rich cathode mMaterials for Li-Ion batteries, Adv. Energy Mater. 8 (2018) 1702397.
[7] I. Bloom, L. Trahey, A. Abouimrane, I. Belharouak, X. Zhang, Q. Wu, W. Lu, D. Abraham, M. Bettge, J. Elam, X. Meng, A. Burrell, C. Ban, R. Tenent, J. Nanda, N. Dudney, Effect of interface modifications on voltage fade in 0.5 Li_2MnO_3· 0.5 $LiNi_{0.375}Mn_{0.375}Co_{0.25}O_2$ cathode materials, J. Power Sources 249 (2014) 509-514.
[8] P. Oh, S. Myeong, W. Cho, M. J. Lee, M. Ko, H. Y. Jeong, J. Cho, Superior long-term energy retention and volumetric energy density for Li-rich cathode materials, Nano Lett. 14 (2014) 5965-5972.
[9] J. Liu, M. Hou, J. Yi, S. Guo, C. Wang, Y. Xia, Improving the electrochemical performance of layered lithium-rich transition-metal oxides by controlling the structural defects, Energy & Environ. Sci. 7 (2014) 705-714.
[10] P. K. Nayak, J. Grinblat, M. Levi, E. Levi, S. Kim, J. W. Choi, D. Aurbach, Al doping for mitigating the capacity fading and voltage decay of layered Li and Mn-rich cathodes for Li-Ion batteries, Adv. Energy Mater. 6 (2016) 1502398.
[11] X. Yang, D. Wang, R. Yu, Y. Bai, H. Shu, L. Ge, H. Guo, Q. Wei, L. Liu, X. Wang, Suppressed capacity/voltage fading of high-capacity lithium-rich layered materials via the design of heterogeneous distribution in the composition, J. Mater. Chem. A 2 (2014) 3899-3911.

[12] J. T. Li, Z. Y. Wu, Y. Q. Lu, Y. Zhou, Q. S. Huang, L. Huang, S. G. Sun, Water-soluble binder, an electrochemical performance booster for electrode materials with high energy density, Adv. Energy Mater. 7 (2017) 1701185.
[13] J. Li, R. Klöpsch, S. Nowak, M. Kunze, M. Winter, S. Passerini, Investigations on cellulose-based high voltage composite cathodes for lithium ion batteries, J. Power Sources 196 (2011) 7687-7691.
[14] S. Zhang, H. Gu, H. Pan, S. Yang, W. Du, X. Li, M. Gao, Y. Liu, M. Zhu, L. Ouyang, D. Jian, F. Pan, A novel strategy to suppress capacity and voltage fading of Li- and Mn-rich layered oxide cathode material for lithium-ion batteries, Adv. Energy Mater. 7 (2017) 1601066.
[15] S. J. Zhang, Deng, Y. P.; Wu, Q. H.; Zhou, Y.; Li, J. T.; Wu, Z. Y.; Yin, Z. W.; Lu, Y.; Shen, C.; Huang, L.; Sun, S. G. Sodium-alginate-based binders for lithium-rich cathode materials in lithium-ion batteries to suppress voltage and capacity fading. ChemElectroChem 2018, 5, 1321-1329.
[16] J. Liu, Q. Zhang, T. Zhang, J. T. Li, L. Huang, S. G. Sun, A robust ion-conductive biopolymer as a binder for Si anodes of lithium-ion batteries, Adv. Funct. Mater. 25 (2015) 3599-3605.
[17] Y. Q. Lu, J. T. Li, X. X. Peng, T. Zhang, Y. P. Deng, Z. Y. Wu, L. Deng, L. Huang, X. Zhou, S. G. Sun, Achieving high capacity retention in lithium-sulfur batteries with an aqueous binder, Electrochem. Commun.72 (2016) 79-82.
[18] T. Zhang, J. T. Li, J. Liu, Y. P. Deng, Z. G. Wu, Z. W. Yin, D. Guo, L. Huang, S. G. Sun, Suppressing the voltage-fading of layered lithium-rich cathode materials via an aqueous binder for Li-ion batteries, Chem. Commun. 52 (2016) 4683-4686.
[19] M. Gu, I. Belharouak, J. Zheng, H. Wu, J. Xiao, A. Genc, A. Amine, S. Thevuthasan, D. Baer, J. Zhang, N. D. Browning, J. Liu, C. Wang, Formation of the spinel phase in the layered composite cathode used in Li-ion batteries, ACS nano 7 (2013) 760-767.
[20] D. Mohanty, J. Li, D. P. Abraham, A. Huq, E. A. Payzant, D. L. Wood III, C. Daniel, Unraveling the voltage-fade mechanism in high-energy-density lithium-ion batteries: origin of the tetrahedral cations for spinel conversion, Chem. Mater. 26 (2014) 6272-6280.
[21] T. Zhang, J. T. Li, J. Liu, Y. P. Deng, Z. G. Wu, Z. W. Yin, J. H. Wu, L. Huang, S.

G. Sun, Improving the electrochemical performance of $Li_{1.14}Ni_{0.18}Mn_{0.62}O_2$ by modulating structure defects via a molten salt method, ChemElectroChem 3 (2016) 98-104.
[22] Z. W. Yin, Z. G. Wu, Y. P. Deng, T. Zhang, H. Su, J. C. Fang, B. Xu, J. Wang, J. T. Li, L. Huang, X. D. Zhou, S. G. Sun. A synergistic effect in a composite cathode consisting of spinel and layered structures to increase the electrochemical performance for Li-Ion batteries. The J. Phys. Chem. C 120 (2016) 25647-25656.
[23] J. H. Kim, N. P. Pieczonka, L. Yang, Challenges and approaches for high-voltage spinel lithium-Ion batteries, ChemPhysChem 15 (2014) 1940-1954.
[24] A. Manthiram, K. Chemelewski, E. S. Lee, A perspective on the high-voltage $LiMn_{1.5}Ni_{0.5}O_4$ spinel cathode for lithium-ion batteries, Energy & Environ. Sci. 7 (2014) 1339-1350.
[25] S. Xu, G. Luo, R. Jacobs, S. Fang, M. K. Mahanthappa, R. J. Hamers, D. Morgan, Ab initio modeling of electrolyte molecule ethylene carbonate dDecomposition rReaction on Li(Ni, Mn, Co)O_2 cathode surface, ACS Appl. Mater. & Interfaces 9 (2017) 20545-20553.
[26] Z. Li, F. Du, X. Bie, D. Zhang, Y. Cai, X. Cui, C. Wang, G. Chen, Y. Wei, Electrochemical kinetics of the $Li[Li_{0.23}Co_{0.3}Mn_{0.47}]O_2$ cathode material studied by GITT and EIS, J. Phys. Chem. C 114 (2010) 22751-22757.
[27] K. Edström, T. Gustafsson, J. O. Thomas, The cathode–electrolyte interface in the Li-ion battery, Electrochim. Acta 50 (2004) 397-403.
[28] Pan, J.; Xu, G.; Ding, B.; Han, J.; Dou, H.; Zhang, X. Enhanced electrochemical performance of sulfur cathodes with a water-soluble binder. RSC Adv. 2015, 5, 13709-13714.
[29] Z. W. Yin, X. Peng, J. Li, C. Shen, Y. Deng, Z. Wu, T. Zhang, Q. Zhang, Y. Mo, K. Wang, L. Huang, H. Zheng, S. G. Sun, Revealing of the activation pathway and cathode electrolyte interphase evolution of Li-rich $0.5Li_2MnO_3•0.5LiNi_{0.3}Co_{0.3}Mn_{0.4}O_2$ cathode by in-situ electrochemical quartz crystal microbalance, ACS Appl. Mater. & Interfaces 11 (2019) 16214−16222.
[30] W. Huang, L. Xing, Y. Wang, M. Xu, W. Li, F. Xie, S. Xia, 4-(Trifluoromethyl)-benzonitrile: a novel electrolyte additive for lithium nickel manganese oxide cathode of high voltage lithium ion battery, J. Power Sources 267 (2014) 560-565.

[31] J. Li, L. Zhang, L. Yu, W. Fan, Z. Wang, X. Yang, Y. Lin, L. Xing, M. Xu, W. Li, Understanding interfacial properties between Li-rich layered oxide and electrolyte containing triethyl borate, J. Phys. Chem. C 120 (2016) 26899-26907.
[32] Z. Zhang, T. Zeng, Y. Lai, M. Jia, J. Li, A comparative study of different binders and their effects on electrochemical properties of $LiMn_2O_4$ cathode in lithium ion batteries, J. Power Sources 247 (2014) 1-8.
[33] J. Zheng, M. Gu, J. Xiao, P. Zuo, C. Wang, J. G. Zhang, Corrosion/fragmentation of layered composite cathode and related capacity/voltage fading during cycling process, Nano Lett. 13 (2013) 3824-3830.
[34] H. Koga, L. Croguennec, M. Ménétrier, P. Mannessiez, F. Weill, C. Delmas, S. Belin, Operando x-ray absorption study of the redox processes involved upon cycling of the Li-rich layered oxide $Li_{1.20}Mn_{0.54}Co_{0.13}Ni_{0.13}O_2$ in Li ion batteries, J. Phys. Chem. C 118 (2014) 5700-5709.
[35] A. Banerjee, Y. Shilina, B. Ziv, J. M. Ziegelbauer, S. Luski, D. Aurbach, I. C. Halalay, On the oxidation state of manganese ions in Li-ion battery electrolyte solutions, J. Am. Chem. Soc. 139 (2017) 1738-1741.
[36] F. Zheng, C. Yang, X. Xiong, J. Xiong, R. Hu, Y. Chen, M. Liu, Nanoscale surface modification of lithium-rich layered-oxide composite cathodes for suppressing voltage fade, Angew. Chem. Int. Edit. 54 (2015) 13058-13062.
[37] W. Liu, P. Oh, X. Liu, S. Myeong, W. Cho, J. Cho, Countering voltage decay and capacity fading of lithium-rich cathode material at 60 ℃ by hybrid surface protection layers, Adv. Energy Mater. 5 (2015) 1500274.
[38] Q. Wu, S. Ha, J. Prakash, D. W. Dees, W. Lu, Investigations on high energy lithium-ion batteries with aqueous binder, Electrochim. Acta 114 (2013) 1-6.
[39] Y. Y. Zhang, S. J. Zhang, J. T. Li, K. Wang, Y. C. Zhang, Q. Liu, R. Xie, Y. Pei, L. Huang, S. G. Sun, Improvement of electrochemical properties of P2-type $Na_{2/3}Mn_{2/3}Ni_{1/3}O_2$ sodium ion battery cathode material by water-soluble binders, Electrochim. Acta 298 (2019) 496-504.
[40] M. H. Ryou, S. Hong, M. Winter, H. Lee, J. W. Choi, Improved cycle lives of $LiMn_2O_4$ cathodes in lithium ion batteries by an alginate biopolymer from seaweed, J. Mater. Chem. A 1 (2013) 15224-15229.
[41] H. Liu, D. Qian, M. G. Verde, M. Zhang, L. Baggetto, K. An, Y. Chen, K.

Carroll, D. Lau, M. Chi, G. M. Veith, Y. S. Meng, Understanding the role of NH_4F and Al_2O_3 surface co-modification on lithium-excess layered oxide $Li_{1.2}Ni_{0.2}Mn_{0.6}O_2$. ACS Appl. Mater. & Interfaces 7 (2015)19189-19200.

[42] S. Zhang, H. Gu, H. Pan, S. Yang, W. Du, X. Li, M. Gao, Y. Liu, M. Zhu, L. Ouyang, D. Jian, F. Pan, A novel strategy to suppress capacity and voltage fading of Li- and Mn- rich layered oxide cathode material for lithium-ion batteries. Adv. Energy Mater. 7 (2017) 1601066.

[43] T. Zhao, S. Chen, R. Chen, L. Li, X. Zhang, M. Xie, F. Wu, The positive roles of integrated layered-spinel structures combined with nanocoating in low-cost Li-rich cathode $Li[Li_{0.2}Fe_{0.1}Ni_{0.15}Mn_{0.55}]O_2$ for lithium-ion batteries. ACS Appl. Mater. & Interfaces 6 (2014) 21711-21720.

[44] D. J. Noelle, M. Wang, A. V. Le, Y. Shi, Y. Qiao, Internal resistance and polarization dynamics of lithium-ion batteries upon internal shorting. Appl. Energy 212 (2018) 796-808.

[45] X. Fleury, M. H. Noh, S. Geniès, P. X. Thivel, C. Lefrou, Y. Bultel, Fast-charging of Lithium Iron Phosphate battery with ohmic-drop compensation method: Ageing study. J. Energy Storage 16 (2018) 21-36.

[46] D. Peak, J. T. Sims, D. L. Sparks, Solid-state speciation of natural and alum-amended poultry litter using XANES spectroscopy. Environ. Sci. & Technol. 36 (2002) 4253-4261.

Table and Fig. captions

Table 1. Impedance parameters of $Li_{1.2}Ni_{0.2}Mn_{0.6}O_2$ using PVDF or GG as binder at different potential during first charge at 0.2 C.

Table 2. Impedance parameters of $Li_{1.2}Ni_{0.2}Mn_{0.6}O_2$ using PVDF or GG as binder after different cycles at 0.5 C.

Fig. 1. The electrochemical performance comparison. (a) Initial charge-discharge profile of $Li_{1.2}Ni_{0.2}Mn_{0.6}O_2$ at 0.2 C using PVDF or GG as binder; (b) CV curves of electrodes only consisting of PVDF or GG binder with a scan rate of 0.2 mV s^{-1}. (c) Cyclabiltiy and (d) average discharge voltage of $Li_{1.2}Ni_{0.2}Mn_{0.6}O_2$ at 0.5 C using PVDF or GG as binder.

Fig. 2. The comparison of electrode/electrolyte interfacial properties. (a) Nyquist plots of $Li_{1.2}Ni_{0.2}Mn_{0.6}O_2$ before cycling using PVDF or GG as binder, and the equivalent circuit model for EIS tests is inserted; (b) The evolution of R_{CEI} of $Li_{1.2}Ni_{0.2}Mn_{0.6}O_2$ at different first-charge potential, and PVDF or GG was used as binder respectively; Nyquist plots of $Li_{1.2}Ni_{0.2}Mn_{0.6}O_2$ after different cycles at 0.5 C using (c) PVDF and (d) GG as binder.

Fig. 3. The electrode morphology comparison. SEM images of $Li_{1.2}Ni_{0.2}Mn_{0.6}O_2$ electrodes before cycling (a) using PVDF binder (b) using GG binder, and after 50 cycles at 0.5 C (c) using PVDF binder (d) using GG binder.

Fig. 4. The microstructure comparison. TEM images of $Li_{1.2}Ni_{0.2}Mn_{0.6}O_2$ material after 50 cycles at 0.5 C using (a, b) PVDF and (c, d) as binder.

Fig. 5. The comparison of valence state and local structure of Mn element in $Li_{1.2}Ni_{0.2}Mn_{0.6}O_2$ during first cycle. *Ex*-situ Mn K-edge XANES spectra of $Li_{1.2}Ni_{0.2}Mn_{0.6}O_2$ during first charge at 0.2 C using (a) PVDF (d) GG as binder. (b) (e) are local enlarged images of region A of (a) (c) respectively. (c) (f) are local enlarged images of region B of (a) (c) respectively. An enlarged image of peak in (f) is insert.

Fig. 6. The comparison of valence state and local structure of Mn element in $Li_{1.2}Ni_{0.2}Mn_{0.6}O_2$ after different cycles. *Ex*-situ Mn K-edge XANES spectra of $Li_{1.2}Ni_{0.2}Mn_{0.6}O_2$ after different cycles at 0.5 C using (a) PVDF (d) GG as binder. (b) (e) are local enlarged images of region A of (a) (c) respectively. (c) (f) are local enlarged images of region B of (a) (c) respectively.

Scheme 1. Role of (a) PVDF and (b) GG binder in charge-discharge process of $Li_{1.2}Ni_{0.2}Mn_{0.6}O_2$ material. Comparing with commercial PVDF binder, GG binder provides stable cathode electrolyte interphase (CEI), inhibits electrolyte decomposition, particles etching and surface structural transformation.

Table 1. Impedance parameters of $Li_{1.2}Ni_{0.2}Mn_{0.6}O_2$ using PVDF or GG as binder at different potential during first charge at 0.2 C.

PVDF		OCP	3.5 V	3.7 V	3.9 V	4.1 V	4.3 V	4.4 V	4.5 V	4.6 V	4.7 V	4.8 V
	R_S	3.78	3.73	3.82	3.88	3.82	3.89	3.74	3.79	4.02	4.01	3.99
	R_{CEI}	211.8	157.3	140.6	126.7	116.1	136.1	176.3	199.4	200.9	220.1	223.2
GG		OCP	3.5 V	3.7 V	3.9 V	4.1 V	4.3 V	4.4 V	4.5 V	4.6 V	4.7 V	4.8 V
	R_S	2.38	2.23	2.27	2.20	2.12	2.23	2.09	2.46	2.25	2.46	2.73
	R_{CEI}	82.6	77.7	74.8	72.7	73.1	73.9	73.2	74.6	75.7	78.5	84.2

Table 2. Impedance parameters of $Li_{1.2}Ni_{0.2}Mn_{0.6}O_2$ using PVDF or GG as binder after different cycles at 0.5 C.

PVDF		OCP	25th	50th	75th
	R_S	3.79	7.15	25.05	9.81
	R_{CEI}	211.8	454.8	530.9	831.1
GG		OCP	25th	50th	75th
	R_S	2.38	3.44	3.85	3.43
	R_{CEI}	82.6	96.7	91.3	86.4

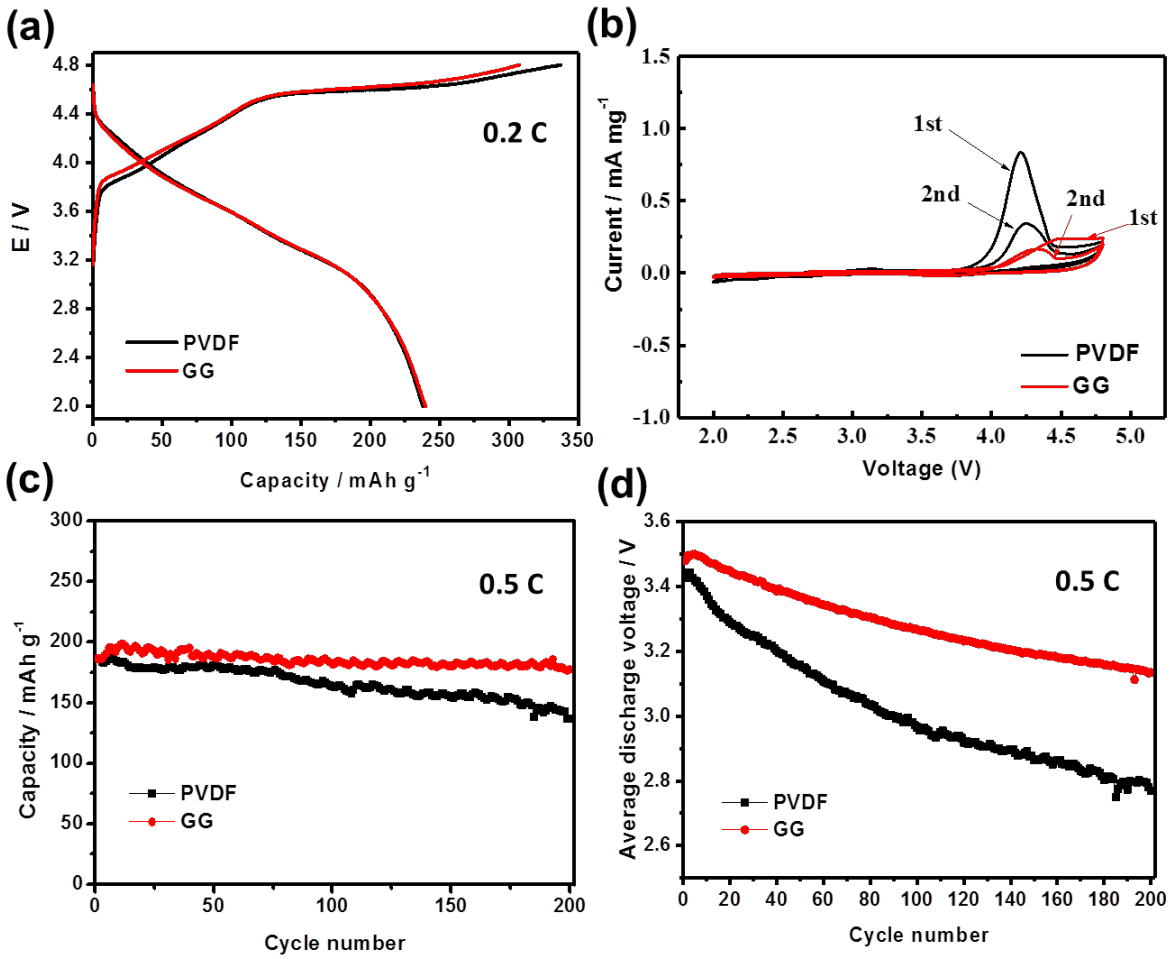

Fig. 1. The electrochemical performance comparison. (a) Initial charge-discharge profile of $Li_{1.2}Ni_{0.2}Mn_{0.6}O_2$ at 0.2 C using PVDF or GG as binder; (b) CV curves of electrodes only consisting of PVDF/GG binder and carbon black (1:1 in weight ratio) on Al current collector with a scan rate of 0.2 mV s^{-1}. (c) Cyclabiltiy and (d) average discharge voltage of $Li_{1.2}Ni_{0.2}Mn_{0.6}O_2$ at 0.5 C using PVDF or GG as binder.

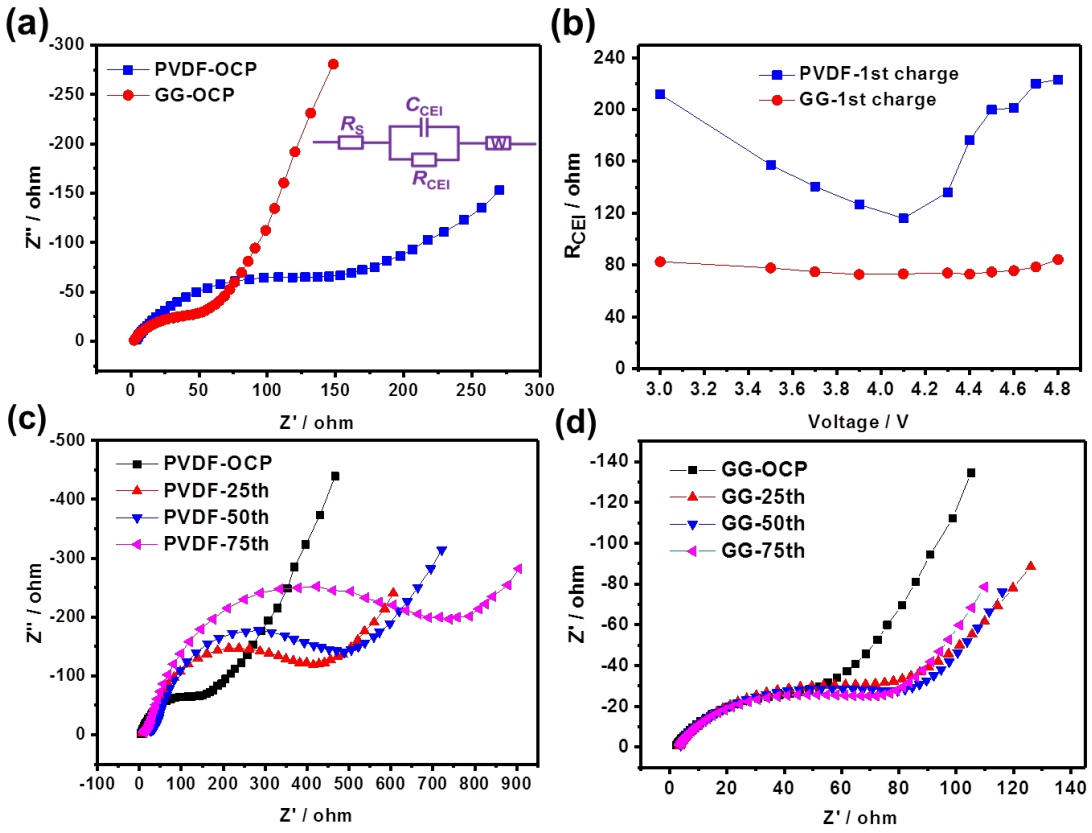

Fig. 2. The comparison of electrode/electrolyte interfacial properties. (a) Nyquist plots of $Li_{1.2}Ni_{0.2}Mn_{0.6}O_2$ before cycling using PVDF or GG as binder, and the equivalent circuit model for EIS tests is inserted; (b) The evolution of R_{CEI} of $Li_{1.2}Ni_{0.2}Mn_{0.6}O_2$ at different first-charge potential, and PVDF or GG was used as binder respectively; Nyquist plots of $Li_{1.2}Ni_{0.2}Mn_{0.6}O_2$ after different cycles at 0.5 C using (c) PVDF and (d) GG as binder.

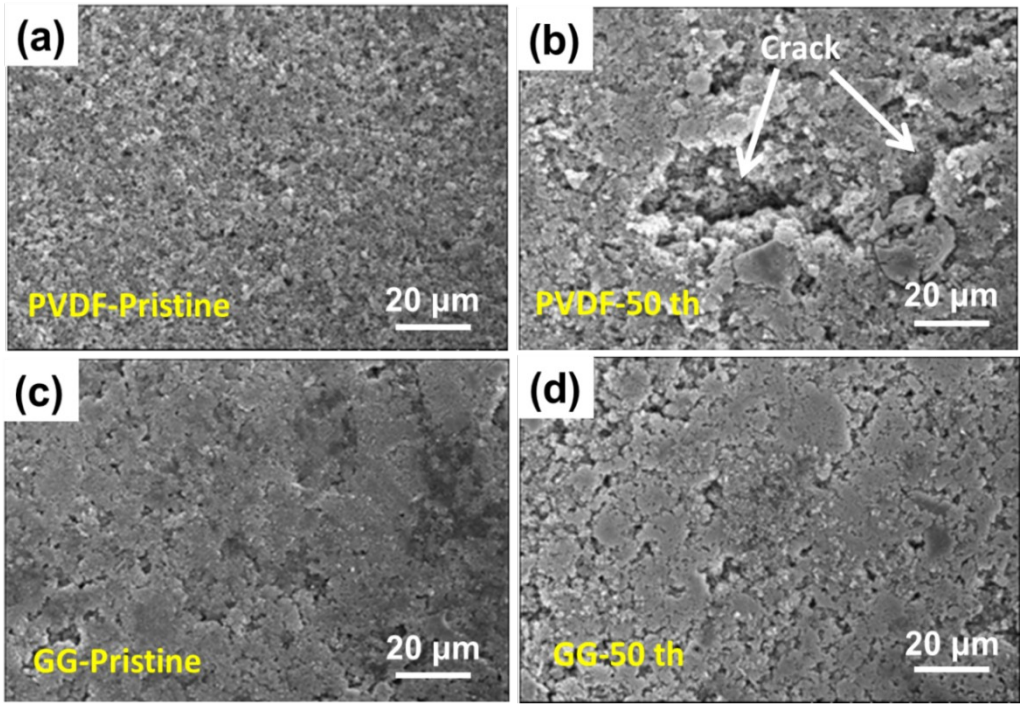

Fig. 3. The electrode morphology comparison. SEM images of $Li_{1.2}Ni_{0.2}Mn_{0.6}O_2$ electrodes before cycling (a) using PVDF binder (b) using GG binder, and after 50 cycles at 0.5 C (c) using PVDF binder (d) using GG binder.

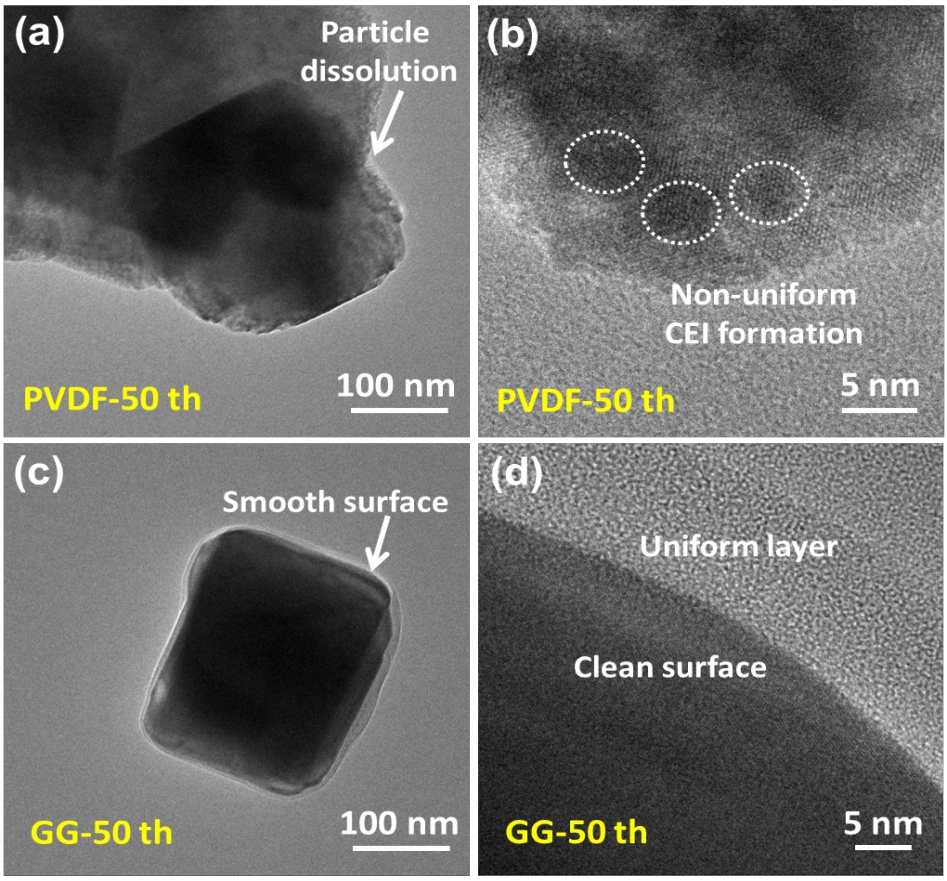

Fig. 4. The microstructure comparison. TEM images of $Li_{1.2}Ni_{0.2}Mn_{0.6}O_2$ material after 50 cycles at 0.5 C using (a, b) PVDF and (c, d) as binder.

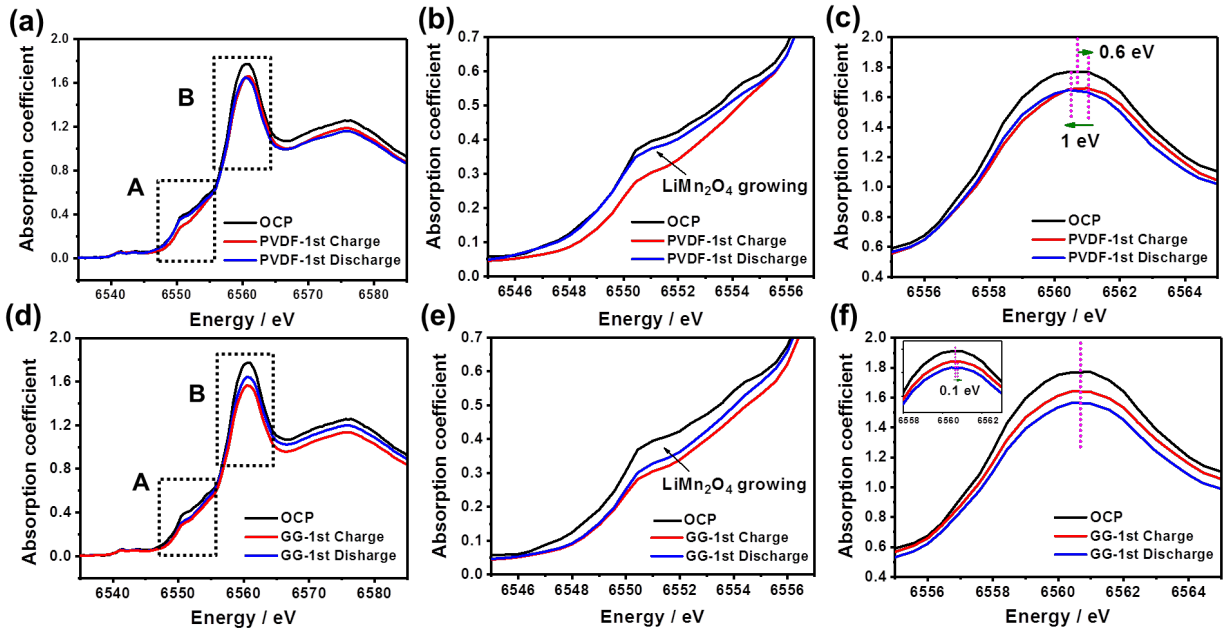

Fig. 5. The comparison of valence state and local structure of Mn element in $Li_{1.2}Ni_{0.2}Mn_{0.6}O_2$ during first cycle. *Ex*-situ Mn K-edge XANES spectra of $Li_{1.2}Ni_{0.2}Mn_{0.6}O_2$ during first charge at 0.2 C using (a) PVDF (d) GG as binder. (b) (e) are local enlarged images of region A of (a) (c) respectively. (c) (f) are local enlarged images of region B of (a) (c) respectively. An enlarged image of peak in (f) is insert.

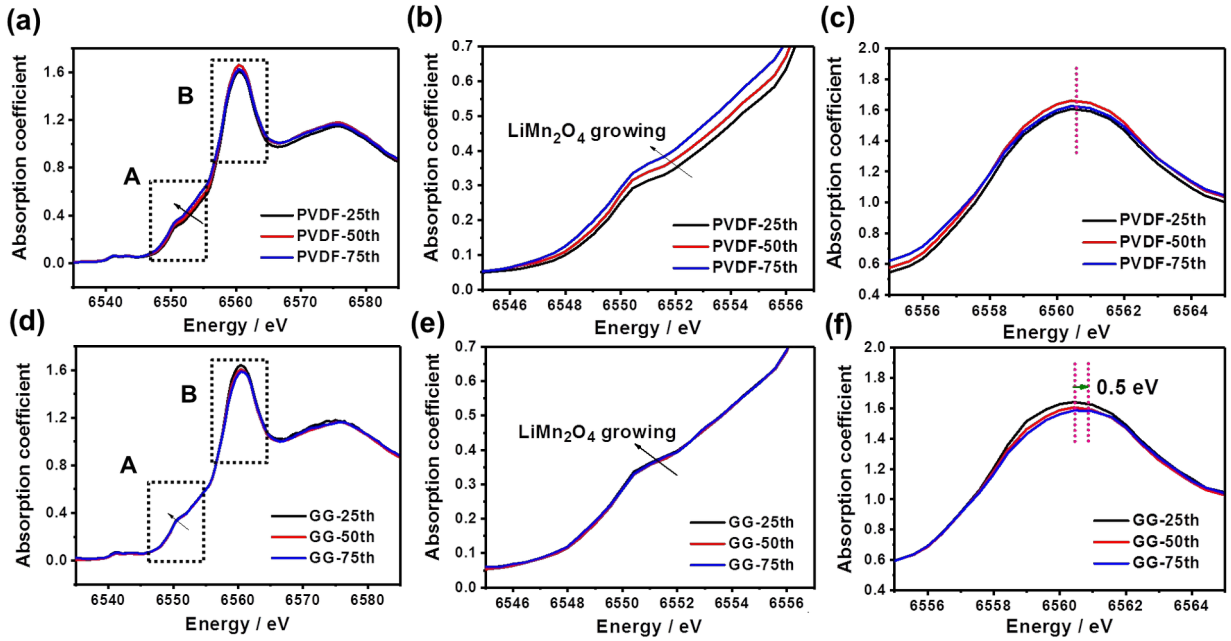

Fig. 6. The comparison of valence state and local structure of Mn element in $Li_{1.2}Ni_{0.2}Mn_{0.6}O_2$ after different cycles. *Ex*-situ Mn K-edge XANES spectra of $Li_{1.2}Ni_{0.2}Mn_{0.6}O_2$ after different cycles at 0.5 C using (a) PVDF (d) GG as binder. (b) (e) are local enlarged images of region A of (a) (c) respectively. (c) (f) are local enlarged images of region B of (a) (c) respectively.

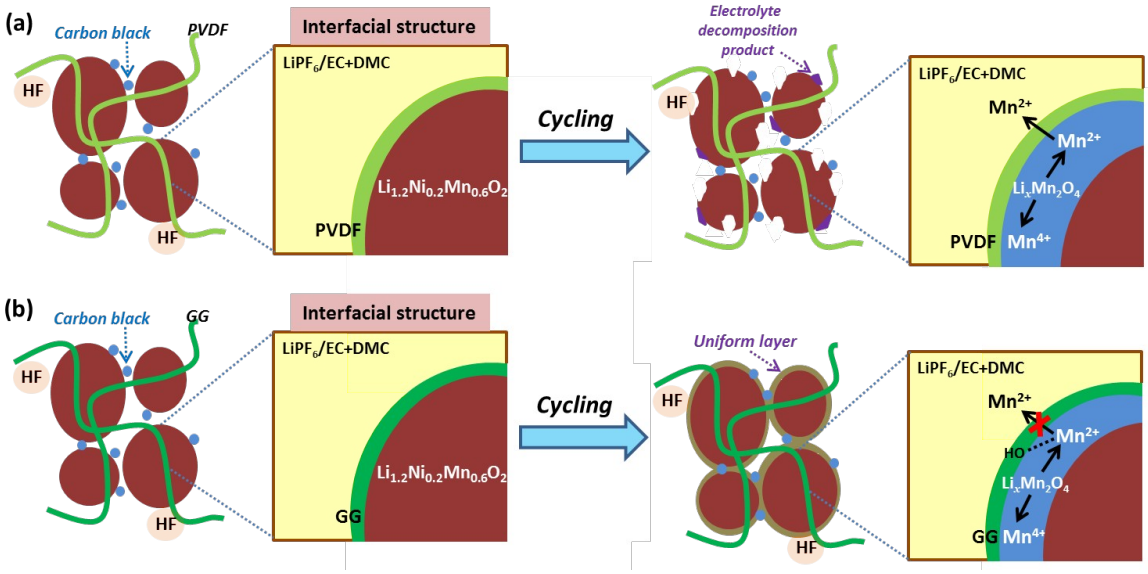

Scheme 1. Role of (a) PVDF and (b) GG binder in charge-discharge process of $Li_{1.2}Ni_{0.2}Mn_{0.6}O_2$ material. Comparing with commercial PVDF binder, GG binder provides stable cathode electrolyte interphase (CEI), inhibits electrolyte decomposition, particles etching and surface structural transformation.